Earth and Planetary Science Letters 389 (2014) 221–229

Contents lists available at ScienceDirect

Earth and Planetary Science Letters

www.elsevier.com/locate/epsl

Dynamic versus flexural controls of Late Cretaceous Western Interior Basin, USA

Shaofeng Liu [a,*], Dag Nummedal [b], Michael Gurnis [c]

[a] State Key Laboratory of Geological Processes and Mineral Resources and School of Geosciences and Resources, China University of Geosciences (Beijing), Beijing 100083, China
[b] Colorado Energy Research Institute, Colorado School of Mines, Golden, CO 80401, United States
[c] Seismological Laboratory and Division of Geological and Planetary Sciences, California Institute of Technology, Pasadena, CA 91125, United States

ARTICLE INFO

Article history:
Received 30 August 2013
Received in revised form 3 January 2014
Accepted 6 January 2014
Available online xxxx
Editor: T.M. Harrison

Keywords:
dynamic subsidence
flexure subsidence
Farallon plate subduction
Western Interior Basin
Late Cretaceous stratigraphy

ABSTRACT

The United States Cretaceous Western Interior Basin has long been considered a foreland basin, driven by the Sevier thrust and associated basin sediment loads. However, flexural studies demonstrate that this effect exists only within a narrow band in front of the thrust belt. Most of the basin appears to be due to mantle flow-induced dynamic subsidence associated with Farallon plate subduction. Here we show how the components of evolving long-wavelength dynamic subsidence and flexural subsidence created the accommodation space and controlled the stratigraphy across the western United States, based on a correlated stratigraphic section across central Utah and Colorado. These backstripped subsidence data reveal the dynamic-topography driven nature of the Western Interior Basin. The results seem to support that the depocenters track the trough of dynamic subsidence with ca. 18 Myr cycles through time and space and the stratigraphic patterns of large-scale progradation, eastward migration of depocenter, and regional clinoform-like downlap are related with the dynamic subsidence. Interpretation of these data also provides more insights into the repeated, ca. 2 to 6 Myr cycles of thrust-induced subsidence in front of the thrust belt, which control the local eastward progradation of the sand bodies from the thrust belt. The dynamic, flexural subsidence and eustatic sea level changes interacted and controlled the timing and distribution of unconformities. Our work shows how the stratigraphy precisely records the timing, patterns and position of dynamic versus flexural subsidences, and that combination of such data leads to important geophysical discoveries and supplies strict constraints for geodynamic modeling.

1. Introduction

The Late Cretaceous Western Interior Basin (WIB) across North America owes its origin primarily to dynamic subsidence associated with subduction of the Farallon plate beneath Rocky Mountains (Pang and Nummedal, 1995; Liu and Nummedal, 2004; Liu et al., 2005, 2011), creating in the process a very large sedimentary basin due to the downward pull of the subducting plate (Gurnis, 1993; Mitrovica et al., 1989; Burgess et al., 1997; Liu et al., 2008; Spasojevic et al., 2009; Flament et al., 2013). The putative dynamic subsidence of the WIB had a 'wave-like' character propagating eastward at the speed of convergence of the Farallon and overlying North American plates (Liu et al., 2011). This dynamically subsiding basin was about five to ten times wider than the portions of the WIB that also were affected by flexural loading of the Sevier thrust belt (Pang and Nummedal, 1995). It is now well documented that this flexural foreland basin, the short-wavelength subsidence, extends eastward from the Sevier thrust front to a forebulge typically 160–180 km distance (Liu and Nummedal, 2004; Luo et al., 2010). Therefore, the Western Interior Basin in total was much wider than the foreland basin part, with the seaway extending from western Wyoming to central Iowa and Minnesota at its maximum extent, and connecting the Gulf of Mexico to the Arctic Ocean north of Canada. Until now, most research on dynamic subsidence has been focused on the vertical plate movements themselves and their effect on continental freeboards and records of relative sea level changes (e.g. Müller et al., 2008). Clearly, such effects are major, and greatly influence regional stratigraphic architecture. However, the broad sedimentary architecture and large-scale regional stratigraphy (Weimer, 1970) have not yet been fully understood in the context of long-wavelength dynamic subsidence. The long wavelength plus flexural subsidence that created the accommodation space and controlled the stratigraphy across the western United States needs to be unraveled.

This paper will document how subsidence across the WIB progressed as a wave from west to east leaving behind a pattern of basin fill, and test how the dynamic plus flexural subsidence created the accommodation space and controlled the late Cretaceous

* Corresponding author. Tel.: +86 10 82321159; fax: +86 10 82321159.
E-mail address: shaofeng@cugb.edu.cn (S.F. Liu).

0012-821X/$ – see front matter
http://dx.doi.org/10.1016/j.epsl.2014.01.006

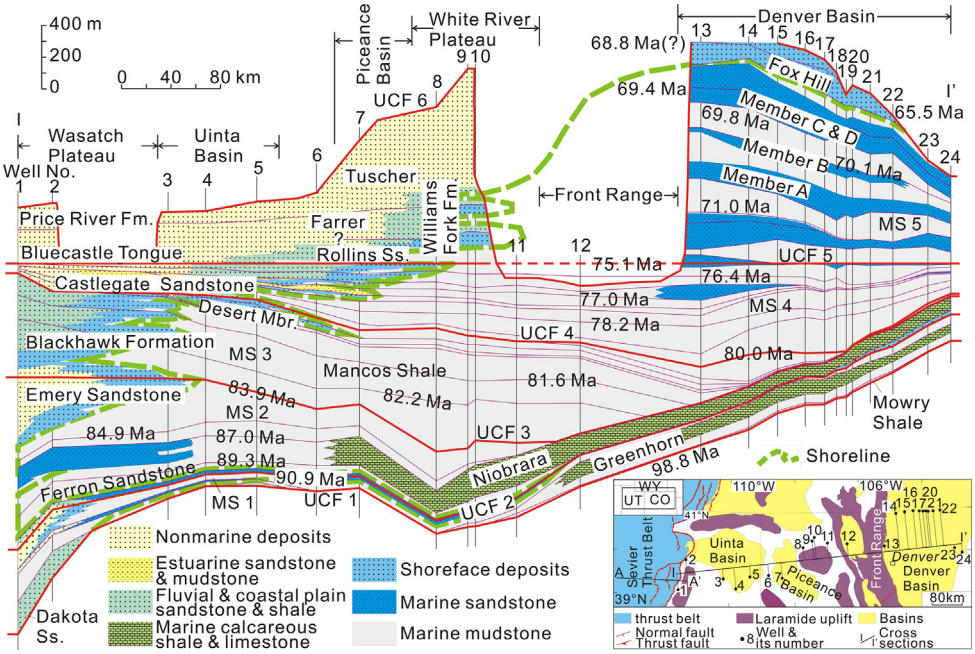

Fig. 1. Regional Upper Cretaceous stratigraphy across UT–CO section based on 24 well logs. The ages are tied to established ammonite biozones and radiometric dates (Gradstein et al., 2004; Cobban et al., 2006). The Cretaceous succession was separated into five megasequences (MS), in which major regional unconformities (UCF) and/or surfaces were chosen as boundaries. Inset map shows segment of Sevier thrust belt and its associated basins in central Rocky Mountain area of United States, in which I–I′ and A–A′ are locations of the stratigraphic and structural sections across Western Interior Basin and Sevier thrust belt, respectively. Fm: Formation; Mbr: Member; Ss: Sandstone. WY: Wyoming; UT: Utah; CO: Colorado.

stratigraphy and unconformities across the western United States over time, based on a correlated stratigraphic section across central Utah and Colorado (UT–CO) (Fig. 1).

2. Differentiation of long-wavelength versus flexural components from total subsidence

The shallow marine sediments of the Late Cretaceous United States WIB are ideal test beds for research on subsidence because they provide unsurpassed bio- (hence chrono-)stratigraphic control (Weimer, 1983; Kiteley, 1978; Fouch et al., 1983; Dyman et al., 1994; Hettinger and Kirschbaum, 2002; Gradstein et al., 2004; Cobban et al., 2006). We constructed a regional cross-section across central Utah (UT)-Colorado (CO) from well logs penetrating the Upper Cretaceous succession (Fig. 1; detailed stratigraphic description in the Supplementary material). The Cretaceous succession was separated into five megasequences (MS), in which major regional unconformities and/or surfaces with rapid changes in subsidence were chosen as the boundaries. A series of stratigraphic intervals have been sequentially decompacted across UT–CO section at ca. 99–91, 91–84, 84–80 and 80–75 Ma show the total cross-sectional subsidence values at different basin phases (Fig. 2; detailed method in the Supplementary material). Overall, the restored basin subsidence patterns demonstrated a systematic temporal evolution, in which the long-wavelength (>500 km) component of the incremental subsidence at the different stages migrated from west to east. Clearly there was a major change in subsidence style above ca. 80 Ma from the previously backward tilting to forward tilting, and the subsidence rate in front of the thrust belt was greatly reduced (Aschoff and Steel, 2011).

Calculation of crustal loading (Pang and Nummedal, 1995; Liu and Nummedal, 2004; Jordan, 1981; Angevine et al., 1990; Flemings and Jordan, 1990) by only the thrust belt (DeCelles and Coogan, 2006) (Fig. 3; detailed method in the Supplementary material) produces asymmetrical cumulative-subsidence curves, with a typical foredeep (ca. 180 km wide) and forebulge that rises above the zero level. To the east of the forebulge there is no detectable subsidence caused by thrust loading. Comparing both of the subsidence curves driven by the thrust load and the thrust plus sediment plus water load suggests that the flexural subsidence at the forebulge and backbulge zones was mainly driven by the sediment-water load, and the subsidence at the foredeep zone driven by both thrust and sediment-water loads. The calculated long-wavelength incremental subsidence, included in the total subsidence, in different incremental stages (ca. 99–91 Ma, 91–84 Ma, 84–80 Ma, and 80–75 Ma) demonstrates a systematic evolution (Liu et al., 2011) (Fig. 4; detailed method in the Supplementary material). The overall width of the long wavelength subsidence zone at any given time is on the order of 600 to 800 km. The maximum subsidence zones migrated eastwards with the shifting rates of 17.6 km/myr from 90.9 to 83.9 Ma, 47.9 km/myr from 83.9 to 80.0 Ma, and 51.2 km/myr from 80.0 to 75.1 Ma along the section. Impressively, these forward shifting rates were variable with a ca. 3-fold rate increasing after ca. 80 Ma compared to the rate of the early stage (Aschoff and Steel, 2011). Taking Wells 8 and 14 as examples, the interval of subsidence in Well 8 from slow during 98.8–90.9 Ma to fast during 90.9–80.0 Ma, and then back to slow during 80.0–75.1 Ma was ca. 18 Myr. The half interval in Well 14 from slow during 83.9–80.0 Ma to fast during 83.9–75.1 Ma was ca. 9 Myr. These subsidence intervals show a ca. 18 Myr of slow-fast-slow cycle, and affected the depositional evolution of the WIB.

3. Dynamic versus flexural controls of Late Cretaceous stratigraphy

Erosion and sedimentary bypass across this wide basin would create unconformities and condensed sections associated with relatively subtle imbalances between the rates of sediment supply and generation of accommodation space. The former would be primarily controlled by shifts in the fluvial delivery systems and climate in the drainage basins, while the latter would be controlled by rates of basin subsidence, which in turn would vary regionally in accordance with the long-wavelength and flexural subsidence mechanisms (Liu and Nummedal, 2004; Liu et al., 2011).

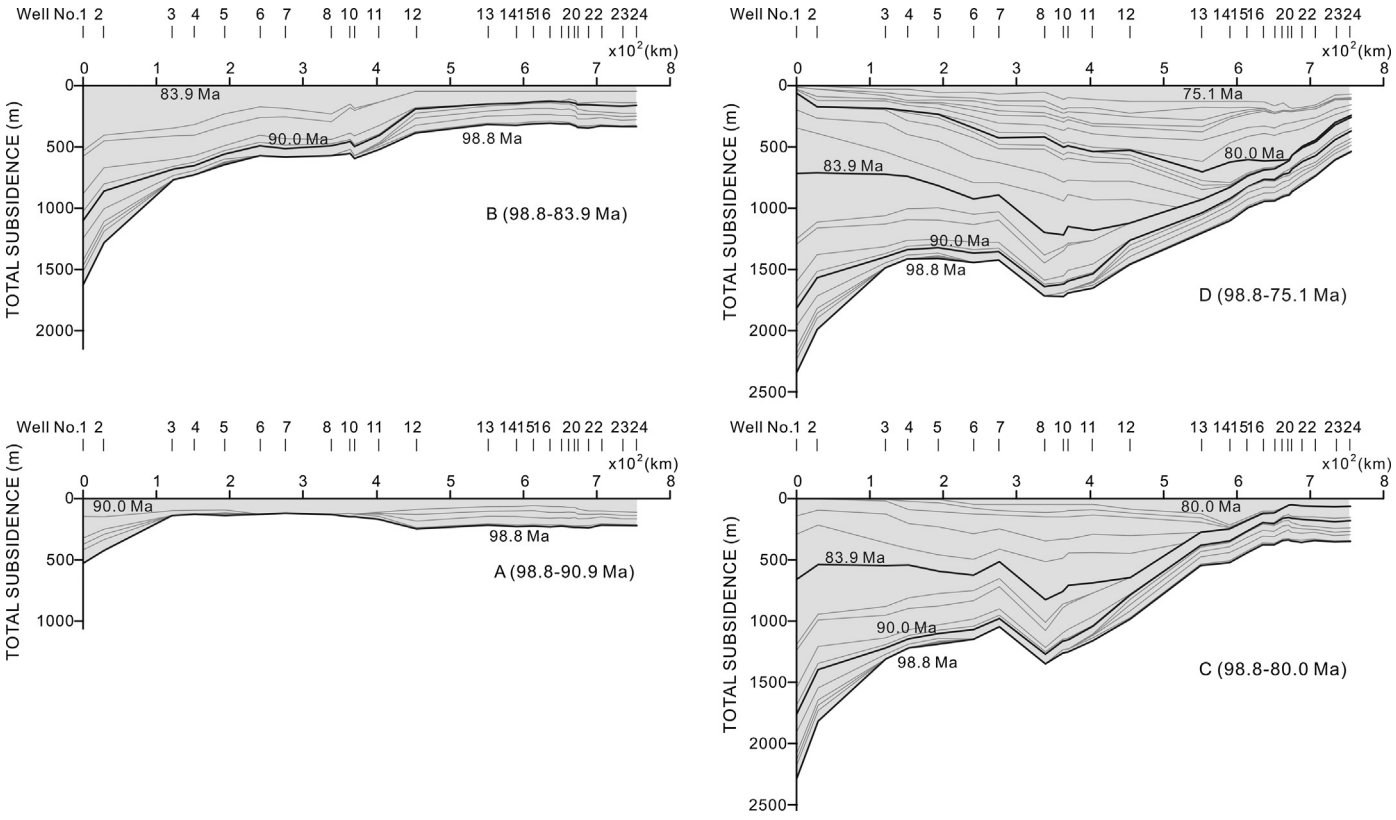

Fig. 2. Two-dimensional cumulative total subsidence history across section I–I′ in Fig. 1 from 98.8 to 75.1 Ma. A series of sequentially restored and decompacted cross-sections at ca. 98.8–90.9 (A), 98.8–83.9 (B), 98.8–80.0 (C), and 98.8–75.1 Ma (D) were developed by setting the eastern ends of the sections as a reference point. The heavy dark lines in the figure represent incremental total subsidence for each successive megasequence interval, and the light grey lines represent the time lines. Restored basin subsidence patterns demonstrated a systematic temporal evolution, in which the long-wavelength (>500 km) component of the incremental subsidence at the different stages migrated from west to east. Location of the section and Wells shown in Fig. 1.

3.1. Stratigraphic response to flexure superimposed on long-wavelength subsidence

The flexural subsidence of Sevier thrust load, superimposed on the pattern of the long-wavelength subsidence, mainly existed in the westernmost part of the section in the west (Fig. 3). The stratigraphy in the depozones of the foredeep and forebulge recorded the events of thrust-related flexural subsidence. Here we differentiate the stratigraphic expression by flexural subsidence of thrust load from present stratigraphic cross-section based on the 1-D basin total subsidence analyses across UT–CO profile (Fig. 5).

The 1-D basin subsidence profiles across UT–CO shows episodes of subsidence at the five MSs (Fig. 5; detailed method in the Supplementary material). The curve segments for ca. 99–91 Ma for the whole section are characterized by relatively rapid subsidence in Wells 1–2 (foredeep), and much slower in Wells 3–10 (forebulge), rapid again in Wells 11–20, and slow again in Wells 21–24 (backbulge) (Figs. 3, 4, and 5), ranging from ca. 101 to 31 m/myr. The subsidence curves of Wells 1 and 2 show that the variation of slow-to-fast-to-slow subsidence rate suggests thrust loading and then unloading events, superimposed on the long-term long-wavelength subsidence interval, active in 98.8–92.7 Ma (ca. 6 Ma short-term interval) and 92.7–90.9 Ma (ca. 2 Ma short-term interval), respectively. The thrust-related subsidence intervals may control the eastward progradation of the sand bodies from the thrust belt (Fig. 6).

Megasequences 2 and 3 are characterized by a ‘classic’ foreland basin subsidence curve (Heller et al., 1986) with one or two segments of slow-to-fast subsidence rate in the western part of the cross-section, representing ca. 3–4 Myr thrust-related events appearing to the west of Well 5 in MS 2 and Well 8 in MS 3 in the foredeep and forebulge depozones (Fig. 5). The zones of maximum rates of subsidence migrated from Well 2 at MS 2 to Well 8 at MS 3, and the rates were ca. 151 and 195 m/myr, respectively. The two subsidence cycles in MS 2 may be related with the two times of progradation of sand bodies to the west of Well 4, but the multiple progradations in MS 3 were developed in one subsidence cycle (Figs. 1 and 6), suggesting there was additive control of sediment supply or eustatic sea-level change events. At the top of MS 3, the shoreface sandstone in the Desert Member progradated into the forebulge depozone in the Piceance basin, which may represent a kind of thrust progradation flexural influence.

The subsidence rates for MSs 4 and 5 in the western parts were slow, nearly constant, and the stratigraphic record is frequently interrupted by unconformities with huge forward accretion rates (Fig. 5). In the east, the subsidence rates were generally high, and they went through a general ‘cycle’ changing from very high rates from 80 Ma to 76 Ma, slower rates from 76 Ma to 71 Ma and then increased again from 71 Ma to the end of the record at 69 Ma. The most rapid subsidence rates of ca. 141 m/myr and ca. 107 m/myr were located at Well 13 and Well 15 in MSs 4 and 5, respectively. The decompacted subsidence curves in the marine shelf deposits in Denver Basin, with a good age-control (Figs. 1 and 6), present a typical slow-to-fast subsidence rate pattern (Fig. 5). The high subsidence rates were only related to eastward-shifting long-wavelength subsidence (Fig. 4).

3.2. Stratigraphic response to long-wavelength subsidence

Long-wavelength subsidence control over the stratigraphy across the WIB is characterized by the eastward migration of the depocenters, large-scale progradation of the continental and

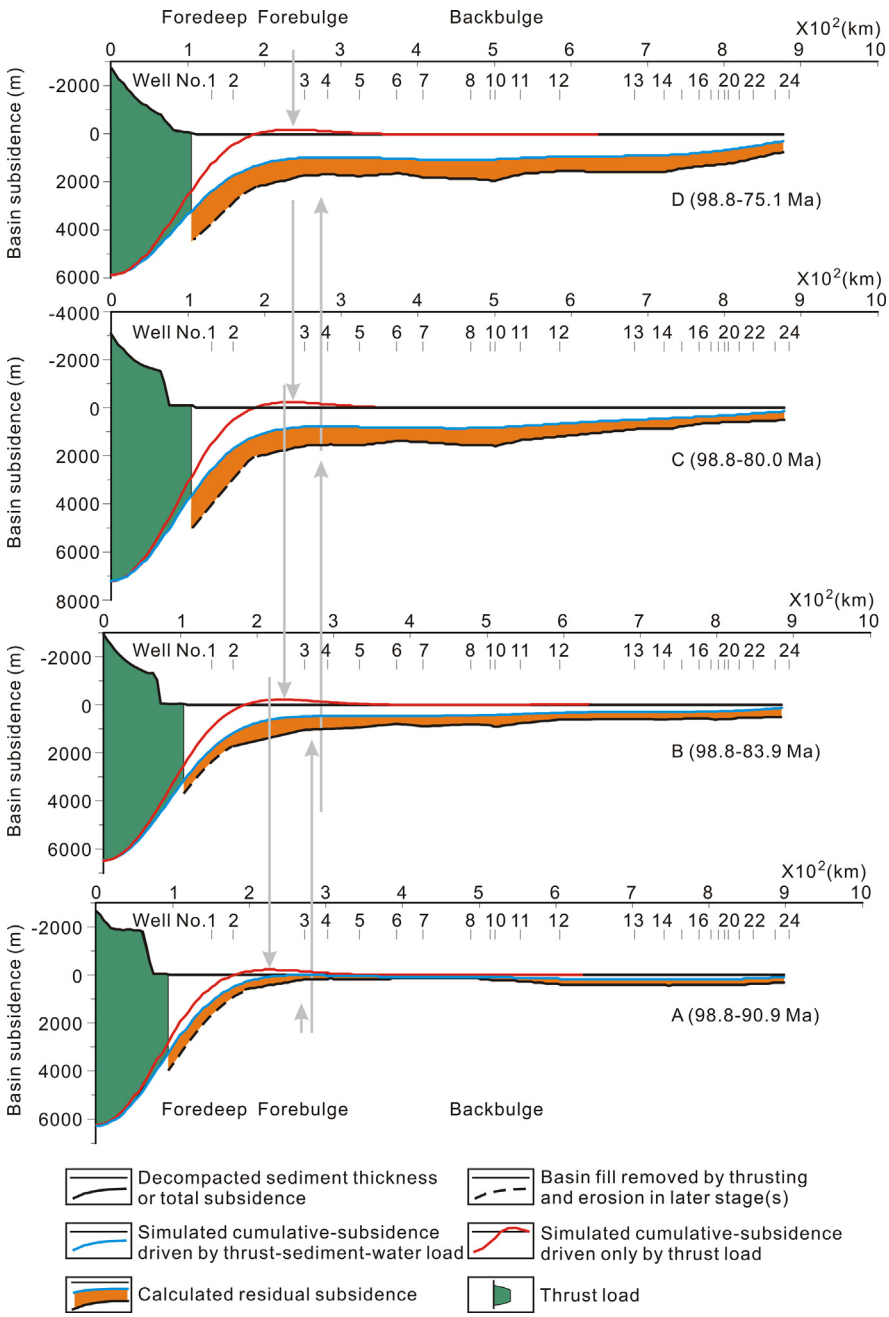

Fig. 3. Flexurally backstripped subsidence profiles across thrust belt and basin of the UT–CO section (section A–A′ and I–I′ in Fig. 1) over four cumulative time intervals of 98.8–90.9 Ma (A), 98.8–83.9 Ma (B), 98.8–80.0 Ma (C), and 98.8–75.1 Ma (D). The regional stratigraphic correlations along the UT–CO section in Fig. 1, and the sequential restoration of the Sevier thrust belt derived from cross-sections in DeCelles and Coogan (2006) (A–A′ section in Fig. 1), allow a precise spatiotemporal subsidence analysis. Calculation of crustal loading suggests that the flexural subsidence at the forebulge and backbulge zones was mainly driven by the sediment-water load, and the subsidence at the foredeep zone driven by both thrust and sediment-water loads. The difference between the total subsidence and the amount of subsidence attributable to flexural loading of both the restored Sevier thrust belt and the WIB sediments (plus water) deposited in the syntectonic stages is referred to as residual subsidence (Liu and Nummedal, 2004). Upper and lower arrows indicate movement of forebulge crest in response to load of thrust belt and load of thrust-sediments-water, respectively. Flexural rigidity used for this calculation was 10^{23} N m. Numbers indicate wells located in Fig. 1.

marine deposits, and regional downlap of the clinoforms. The reconstructed sections of the total subsidence time lines across UT–CO, by choosing the tops of the Greenhorn (ca. 93 Ma) and Niobrara (ca. 87 Ma) Formations as the horizontal base lines, demonstrate a large scale clinoform-like set (Fig. 7), representing a general eastward progradation pattern with regional downlap (Fig. 1). The clinoform-like set between 92.7 and 89.3 Ma downlap onto the Greenhorn limestone top, and the clinoform at 89.3 Ma cumulatively dips 0.034° eastward (Fig. 7A). The depositional systems along these gentle clinoforms progressed from fluvial, through coastal plain, to shallow marine sandstone and mudstones, which suggest that the long-wavelength subsidence locus was mainly located to the west of the section, and the broad marine shale and limestone deposits at the east were developed under the setting of slow long-wavelength subsidence.

The clinoform-like set between 87.0 and 80.0 Ma, downlapping onto the Niobrara Formation top, cumulatively dip at 0.22°, then becoming essentially horizontal as they merge with the top Niobrara Formation (Fig. 7B). Depositional systems were developed with fluvial and coastal plain in their western margin, shallow marine mudstones in the clinoform, and distal mudstones and carbonates at the front (Figs. 1 and 6). This stratigraphic framework

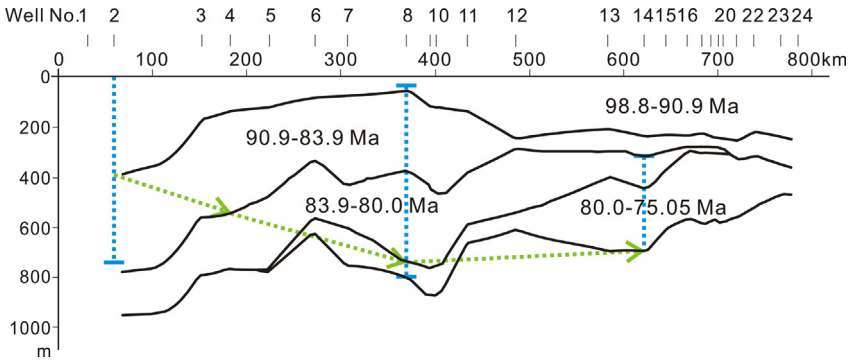

Fig. 4. Profiles of the long-wavelength subsidence differentiated from the backstripped Upper Cretaceous strata, for each time interval, across UT–CO. Incremental subsidence in different incremental stages (ca. 98.8–90.9 Ma, 90.9–83.9 Ma, 83.9–80.0 Ma, and 80.0–75.05 Ma) demonstrates a systematic eastward-migration evolution. Blue dotted lines represent slow-fast-slow subsidence rate cycles at the Well 2, Well 8, and Well 14. Green arrows indicate location and migration of maximum subsidence zones which might be related with the subducted Farallon slab crests under the western United States. Location of the wells is shown in Fig. 1. (For interpretation of the references to color in this figure legend, the reader is referred to the web version of this article.)

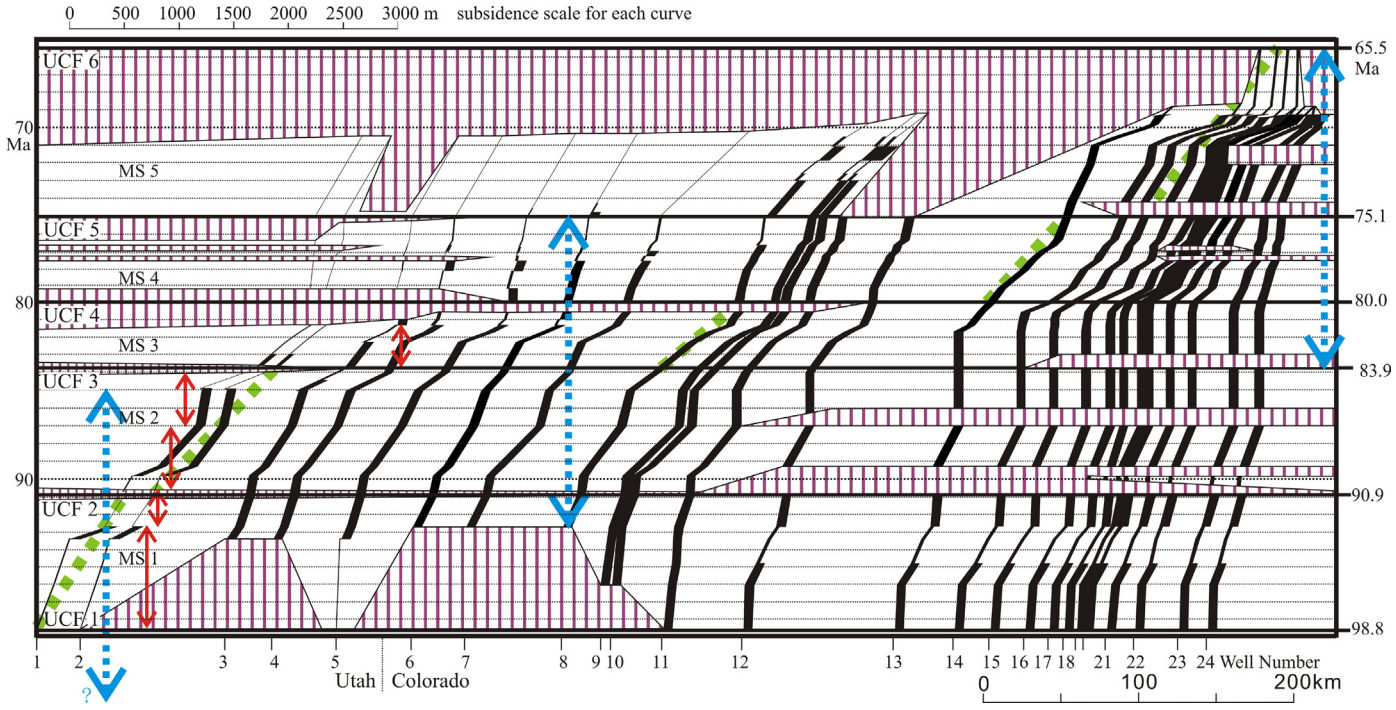

Fig. 5. Total subsidence curves for 24 well sections in UT–CO. Horizontal axis shows well location and distance coordinate for wells (lower), the subsidence scale for each curve (upper); Vertical axis shows ages. The width of the curves represents paleo-bathymetry uncertainty, and the hatched pattern represents hiatuses. The doted green lines indicate the wells with the most rapid subsidence rate in each megasequence, the red arrows represent the "short-term" slow to fast subsidence rate cycles, and blue arrows represent the "long-term" slow-fast-slow subsidence rate cycles. Location of the wells is shown in Fig. 1. (For interpretation of the references to color in this figure legend, the reader is referred to the web version of this article.)

suggests that the long-wavelength subsidence locus was shifted eastward relatively to the early stage, which induced the downlap of clinoform-like set at the eastern front (Figs. 4 and 7B). To the west of Well 7, the sediment supply from the nearby thrust belt was approximately balanced with the level of the subsidence, and the nonmarine, coastal plain and shoreface were deposited and prograded from Wells 1 to 7 with decrease of the long wavelength subsidence rate during ca. 87 and 80 Ma. The area from Wells 7 and 11 was mostly located at the long-wavelength subsidence locus at the stage of ca. 87–80 Ma, and the sediments sourced from western basin margin were under-filled within the maximum subsidence center in the environment of shallow marine. From Wells 11 to 14, where the eastern half of the long-wavelength subsidence zone at the stage of ca. 84–80 Ma was located, the sediments was deposited with marine shale downlapping onto the top of the Niobrara Formation because of gradually eastward shifting of the long-wavelength subsidence zone. From Wells 14 to 24, which was beyond the subsidence zone, the rates of long-wavelength subsidence and sediment supply were all very slow, and then the thin marine shale was deposited (Figs. 6 and 7B).

Further eastward migration of the depocenter in MS 4 and MS 5 strongly suggests that the basin accommodation was mainly driven by the long-wavelength subsidence, not a thrust-induced flexure, and the amplitude of flexural-induced topography strongly decayed beyond the forebulge (Figs. 3 and 4). The eastward onlap and erosional truncation along UCF 4, the multiple unconformities in MS 4, and eastward progradation of the sandbodies shown in its western part may be the response to decrease of the long-wavelength subsidence and migration of the subsidence locus. Especially, there was a spectacular reversal of the stratigraphic thickening from the previous growth toward the thrust belt to the basinward thickening. Detailed regional

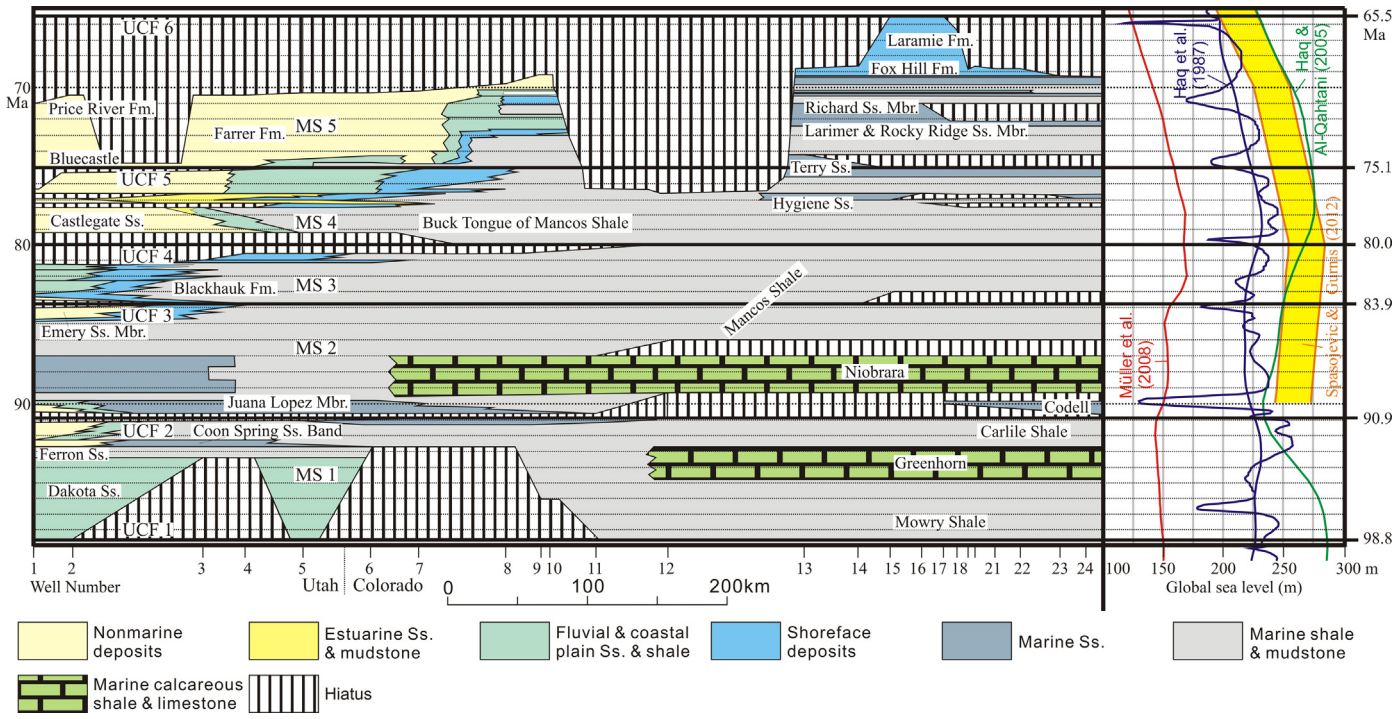

Fig. 6. Time-stratigraphic, unconformity, and global eustatic sea-level correlation chart for the Upper Cretaceous from section I–I′ in Fig. 1. The time-stratigraphic section, with the horizontal axis for well location and distance and the vertical axis for ages, was compiled from the correlation section of Fig. 1. The ages of time-stratigraphic boundaries are based on the Late Cretaceous time scale (Gradstein et al., 2004) and the chronology for the Western Interior Cretaceous (Cobban et al., 2006). Location of the wells is shown in Fig. 1. Eustatic sea-level changes of the North American Late Cretaceous Western Interior are cited from Müller et al. (2008), Haq et al. (1987), Haq and Al-Qahtani (2005), and Spasojevic and Gurnis (2012). UCF: Unconformity; MS: Megasequence.

sequence-stratigraphic correlation by Aschoff and Steel (2011) suggests this dramatic architectural change occurred at 77 Ma, and the extensive (>300–400 km) "sheet-like" amalgamated wedge at this time may have been caused by eastward migration of long-wavelength subsidence. The thick mudstone was deposited between Wells 13 and 20 in MS 4, where the subsidence rate was still high (Fig. 4). The long-wavelength subsidence locus in MS 5 migrated to the Denver Basin (Fig. 1).

3.3. *Interplay of dynamic subsidence, flexure and eustatic sea level changes-expressed by unconformities*

The major unconformities across UT–CO were mapped by the time-stratigraphic correlation (Weimer, 1983; Kiteley, 1978; Fouch et al., 1983; Dyman et al., 1994; Hettinger and Kirschbaum, 2002; Gradstein et al., 2004; Cobban et al., 2006) through identifying truncation, onlap, and downlap of key markers in the subsurface (Fig. 6) (see detailed unconformity description in the Supplementary material). Recognizing the complexity and diversity of mechanisms behind the erosional unconformities in WIB is critical before attributing one particular set of unconformities to any particular mechanism, such as e.g. forebulge uplifts. Fig. 6 is used to evaluate the probability of which particular mechanism may have been dominant in different parts of the basin at different times. Also, the concepts embedded in Fig. 6 do provide a basis for predicting whether any one particular unconformity might become a conformity towards the foredeep in the west (rapid subsidence at certain times) or towards the more distal parts of WIB to the east where we suspect the locus of dynamic subsidence dominated. Depositional sequences bounded by unconformities that become conformable when traced in opposite directions across the basin would not be expected to be correlative, because they are stratigraphic products of different subsidence mechanisms with limited spatial extent.

The Late Cretaceous WIB was generally of low relief, and susceptible to sediment bypass and resulting unconformities in response to dynamic subsidence migration, flexural rebound, and global sea-level change. The locally distributed UCF 1 at the base of MS 1 was likely induced by both forebulge uplift and dynamic subsidence low, even though the sea-level was more than 200 m rise (Fig. 6). This unconformity became conformable eastwards, where there was lack of thrust loading subsidence and the dynamic subsidence was higher. The sea level decreased to the low stand (ca. 230 m (Haq and Al-Qahtani, 2005), ca. 129 m (Müller et al., 2008), and ca. 130 m at the high-frequency curve (Haq et al., 1987)) at ca. 90–91 Ma, which may be the main origin of UCF 2. At the eastern part of UT–CO section (to the east of Well 12), the dynamic subsidence was low, which increased the duration of UCF 2. At the western part of the section, the unconformity may have been strengthened by flexural slowdown. The unconformity at the top of the Niobrara Formation was a downlap unconformity, at which the sea level was steady (Müller et al., 2008; Haq et al., 1987) or slowly increasing (Spasojevic and Gurnis, 2012), but the dynamic subsidence was low. Therefore, the dynamic subsidence was its main driving mechanism. During the time interval (84–80 Ma) the long wavelength subsidence rates increased in UT–CO (Fig. 4). The zone of most rapid subsidence shifted to the middle of UT–CO profile. In addition, the sea level increased from ca. 84 to 80 Ma (Bond, 1978; Haq et al., 1987; Haq and Al-Qahtani, 2005; Müller et al., 2008; Spasojevic and Gurnis, 2012). Therefore, UCF 3 at the base of MS3 was mainly conformable except for a minor unconformity induced by flexural slowdown at the westernmost part of the section and downlap unconformity induced by dynamic low at the easternmost part of the section. During the time interval (ca. 80–75 Ma), the overall dynamic subsidence rates decreased. The center of long-wavelength subsidence along UT–CO section shifted east to the Denver basin where the subsidence rates still remained high (ca. 61 m/Ma)

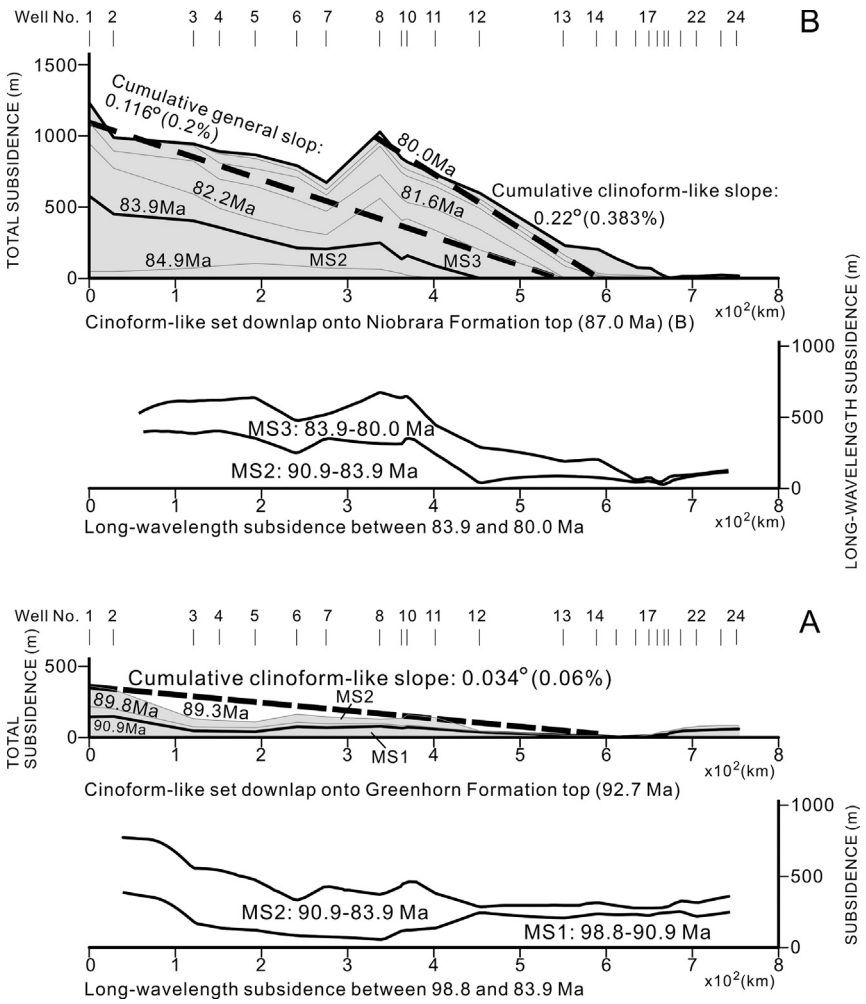

Fig. 7. Large scale clinoform-like sets and their comparative with the long-wavelength subsidence across UT–CO. (A) The clinoform-like sets downlapping onto the top of the Greenhorn Formation and the long-wavelength subsidence between 98.8 and 83.9 Ma. (B) The clinoform-like sets downlapping onto the top of the Niobrara Formation and the long-wavelength subsidence between 83.9 and 80.0 Ma. The heavy dark lines in the figure represent megasequence boundaries, the heavy dark dashed lines represent the slopes of clinoforms, and the light grey lines represent the time lines.

(Fig. 4) (Liu et al., 2011). The global sea level reached high stand at ca. 80 Ma, but began to slowly decrease afterward (Bond, 1978; Haq et al., 1987; Haq and Al-Qahtani, 2005; Müller et al., 2008; Spasojevic and Gurnis, 2012). Therefore, UCF 4 and the multiple localized unconformities within MS4 at the westernmost part of the section might be due to a long-wavelength subsidence locus migrating eastward and the thrusting slowdown (Fig. 6). Due to this tectonic uplift, downcutting of the Castlegate river channels occurred along UCF 4 (Aschoff and Steel, 2011). The unconformities at the easternmost part of the section were downlap unconformities which have been driven by dynamic subsidence. During the time interval (ca. 75–66 Ma), the Denver basin still kept high subsidence, but its locus moved to Wyoming Wind River Basin due to the underlying Farallon plate migration northeastwards (Liu et al., 2008). Sevier thrusting was slowed or became quiescent, and there was no significant crustal thickening (DeCelles and Coogan, 2006), which might induce crustal rebounding uplift at the western part of UT–CO section. In addition, the global sea-level decreased since ca. 75 Ma (Bond, 1978; Haq et al., 1987; Haq and Al-Qahtani, 2005; Müller et al., 2008; Spasojevic and Gurnis, 2012). So, UCFs 5 and 6 and the unconformities between them were induced by dynamic uplift, flexural rebound, and sea-level changes in the westernmost part, and dynamic subsidence low and sea level changes in the middle and the east. Therefore, Interpretation of the stratigraphy provides insight on the dynamic and flexural driven-mechanism of subsidence and deposition with an influence of global eustatic sea level changes in the WIB of the United States.

4. Discussion

The 1-D basin subsidence profiles show that both of the long-wavelength and flexural subsidence signals are superimposed (Fig. 5). The four intervals of fast subsidence rates at ca. 93.4–92.7 Ma, ca. 90–87 Ma, ca. 85–84 Ma, and ca. 82.2–81.2 Ma, expressed in Wells 1 to 4, may be correlated with the major thrust events in the Sevier thrust belt (DeCelles and Coogan, 2006; DeCelles, 2004). These ‘short-term’ subsidence intervals did not exist farther east, instead, the “long-term” slow-fast-slow cycles exist along the whole section. Superimposed on the thrust load cycles in the far west (Wells 1 to 4), the “long-term” subsidence cycle lasted for ca. 14 Myr (99 to 85 Ma), then this “long-term” cycle shifted eastward, and lasted from ca 93 to 75 Ma in wells 5–12. Afterwards, the long-wavelength subsidence shifted even farther east and its cycle showed up very well in Wells 13 to 24, lasting from ca. 84 Ma to 65 Ma. These “long-term” subsidence cycles in ca. 18 Myr were consistent to those of the long-wavelength subsidence shown in Fig. 4.

Consequently, a spatially limited trough of high subsidence rates in front of the thrust belt affected sediment accumulation rates and stratigraphic patterns only across the westernmost about

15% of the WIB (Fig. 6). Along the western margin of this seaway basin there were extensive alluvial and coastal plain deposits extending westward to the Sevier thrust belt (Aschoff and Steel, 2011). Many river systems originated in the high Sevier mountain belt further west, passing through the fringing thrust belt on their way to the seaway. These wide alluvial and coastal plain deposits in the western part of WIB filled the accommodation space, with an approximately balanced, aggradational sandstone wedge with wide low relief before ca. 80 Ma (Hampson et al., 2012). Afterwards, the fluvial clastic wedges (Castlegate and Bluecastle river systems) above UCFs 4 and 5 are highly progradational. Aschoff and Steel (2011) suggested this rapid and extensive progradation of clastic wedges was facilitated by reduced subsidence during the transition from Sevier- to Laramide-style deformation.

Long-wavelength subsidence control over the stratigraphy across the WIB discussed above is characterized by the eastward migration of the depocenters, large-scale progradation of the continental and marine deposits, and regional clinoform-like downlap (Figs. 1, 6, and 7). The long-wavelength subsidence may be the regional dynamic subsidence induced by Farallon slab subduction under the North America (Liu et al., 2008, 2011). The clinoform-like architecture reflects the dynamic subsidence, gradually decreasing towards both the east and west with a half-width of more than 250 km, moved away from the subduction zone along the western margin of the continent. The dominant clastic systems feeding the eastward-prograding clinoform-like sets delivered sediments into the basin along the most rapidly subsiding western margin at first, thus offsetting the rapid subsidence. Farther east with time, where sediment accumulation rates were less, but the dynamic subsidence rate was high with its loci shift eastwards. As a result, the geometry of the observed clinoform-like sets was controlled by the sediment dispersal processes, with regional dynamic subsidence patterns also playing an important role.

The zone of maximum dynamic subsidence, associated with the position of the crest of the underlying, subsiding Farallon slab (Liu et al., 2011), moved eastward about 700 km from 100 Ma to 75 Ma. The rates associated with this dynamic component ranged from a high 150 m/myr above the slab crest to less than a 20 m/myr several hundred kilometers away. The flexural subsidence component also moved eastward over time, but over a much shorter distance, because the Sevier thrust front itself moved less than 100 km during its life (DeCelles and Coogan, 2006). The rates of flexural subsidence were high near the thrust belt, as much as 300 m/myr, but then decreased rapidly eastward to a zone of slow uplift at the forebulge. The thrust-related foredeep will rebound during quiescence periods between thrust movements (as the load of the mountain belt gets redistributed by erosion and transport) with ca. 2–6 Ma cycles, whereas dynamic subsidence was a one-way street, down, as the subducting slab took its place beneath the subsidence center, and was slowdown, as the slab passed away, during ca. 18 million years during the Late Cretaceous. Another contributor to sediment accommodation and removal in the WIB was global sea level change. The widespread clastic wedges at the western margin of the basin can be subdivided into several regressive–transgressive sequences of 200–400 kyr time scale. These fourth-order sequences reflect extensive, repeated regressive–transgressive transits of delta complexes across the shallow-water Western Interior seaway, possible driven mainly by eustasy, although modulated by subsidence and by sediment supply (Gomez-Veroiza and Steel, 2010; Hampson et al., 2011; Aschoff and Steel, 2011). Following several decades of work on sea level variations, the Cretaceous history is now quite well known, although a lively scientific debate accompanies the interpretations (Müller et al., 2008; Spasojevic and Gurnis, 2012). Global sea-level change is mostly thought to result from the changing age distribution of the sea floor, but dynamic topography, emplacement of oceanic plateaus and sedimentation influences the signal (Spasojevic and Gurnis, 2012; Flament et al., 2013). Some of the most detailed data on Late Cretaceous global sea-level changes derive from work by Haq et al. (1987) and Haq and Al-Qahtani (2005); this data set and the predicted global sea-level curves (Müller et al., 2008; Spasojevic and Gurnis, 2012) are used here. The data in Fig. 6 suggest that global eustatic sea-level changes during the Late Cretaceous may have been as high as 300 m. Therefore the three components of dynamic topography, flexure, and eustatic sea level change interacted and controlled the unconformities.

5. Conclusions

The Upper Cretaceous section across UT–CO records how the WIB progressively migrated eastward in response to dynamic subsidence above the subducting Farallon plate (Liu et al., 2011). The subsiding trough was about 600 to 800 km wide, and at any given location the signal of dynamic subsidence lasted about 18 Myr. The transit of the dynamic subsidence trough across the WIB lasted from 100 Ma to 65 Ma. At the western margin of the WIB there was an additional subsidence driver, the Sevier fold-and-thrust belt, which created a ca. 180-km-wide flexural foreland basin with repeated cycles of subsidence, each lasting about 2 to 6 Myr. In this backstripping and tectonic subsidence reconstruction, the two mechanisms are readily differentiated. The sedimentary fill of the long-wavelength dynamic subsidence basin is characterized by the eastward migration of depocenters, progradation of fluvial, coastal plain and marine depositional systems, and downlap at the toes of individual clinoforms. The depocenters track precisely the trough of dynamic subsidence through time and space. The dynamic, flexural subsidence and eustatic sea level changes interacted and controlled the timing and distribution of unconformities. Interpretation of the stratigraphy provides insight on the dynamic and flexuraly-driven mechanism of subsidence and deposition in the Western Interior Basin. Referring to the basin as the "Western Interior Foreland Basin" driven only by the Sevier thrust in the past (Jordan, 1981; Cross and Pilger, 1978; Cross, 1986; DeCelles, 1994), lost much information of the basin formation.

Author contributions

S.F.L. did idea development and data compilation, and wrote main part of the manuscript. D.N. did idea development with S.F.L. and wrote a part of the paper. M.G. joined to interpret a part of the paper and reviewed the paper.

Acknowledgements

We gratefully acknowledge informative discussions with Prof. Ronald Steel. The work was funded by Chinese Natural Science Foundation grants (Nos. 41030318, 91114203), Specialized Research Fund for the Doctoral Program of Higher Education (No. 20130022110002), Colorado Energy Research Institute at Colorado School of Mines. A visiting associate for the senior author at California Institute of Technology was supported by China Scholarship Council and Seismological Lab and Tectonic Observatory (Caltech).

Appendix A. Supplementary material

Supplementary material related to this article can be found online at http://dx.doi.org/10.1016/j.epsl.2014.01.006.

References

Angevine, C.L., Heller, P.L., Paola, C., 1990. Quantitative Sedimentary Basin Modeling. American Association of Petroleum Geologists Shortcourse Note Series, vol. 32.

Aschoff, J., Steel, R., 2011. Anomalous clastic wedge development during the Sevier–Laramide transition, North American Cordilleran foreland basin, USA. Geol. Soc. Am. Bull. 123, 1822–1835.

Bond, G., 1978. Speculations on real sea-level changes and vertical motions of continents at selected times in the Cretaceous and Tertiary periods. Geology 6, 247–250.

Burgess, P.M., Gurnis, M., Moresi, L., 1997. Formation of sequences in the cratonic interior of North America by interaction between mantle, eustatic and stratigraphic processes. Geol. Soc. Am. Bull. 108, 1515–1535.

Cobban, W.A., Obradovich, J.D., Walaszcyk, I., McKinney, K.C., 2006. A USGS zonal table for the Upper Cretaceous Middle Cenomanian–Maastrichtian of the western interior of the United States based on ammonites, inoceramids, and radiometric ages. U.S. Geological Survey Open-File Report 2006-1250. 46 pp.

Cross, T.A., 1986. Tectonic controls of foreland basin subsidence and Laramide style deformation, western United States. In: Allen, P., Homewood, P. (Eds.), Foreland Basins. In: International Association of Sedimentologists Special Publication, vol. 8, pp. 15–39.

Cross, T.A., Pilger Jr., R.H., 1978. Tectonic controls of Late Cretaceous sedimentation, western interior, U.S.A. Nature 274, 653–657.

DeCelles, P.G., 1994. Late Cretaceous–Paleocene synorogenic sedimentation and kinematic history of the Sevier thrust belt, northeast Utah and southwest Wyoming. Geol. Soc. Am. Bull. 106, 32–56.

DeCelles, P.G., 2004. Late Jurassic to Eocene evolution of the Cordilleran thrust belt and foreland basin system, western U.S.A. Am. J. Sci. 304, 105–168.

DeCelles, P.G., Coogan, J.C., 2006. Regional structure and kinematic history of the Sevier fold-and-thrust belt, central Utah. Geol. Soc. Am. Bull. 118, 841–864.

Dyman, T.S., Merewether, E.A., Molenaar, C.M., Cobban, W.A., Obradovich, J.D., Weimer, R.J., Bryant, W.A., 1994. Stratigraphic transects for Cretaceous rocks, Rocky Mountains and Great Plains regions. In: Caputo, M.V., Peterson, J.A., Franczyk, K.J. (Eds.), Mesozoic Systems of the Rocky Mountain Region, USA, Denver, Colorado. Rocky Mountain Section SEPM, pp. 365–392.

Flament, N., Gurnis, M., Müller, R.D., 2013. A review of observations and models of dynamic topography. Lithosphere 5, 189–210.

Flemings, P.B., Jordan, T.E., 1990. Stratigraphic modeling of foreland basins: Interpreting thrust deformation and lithosphere rheology. Geology 18, 430–434.

Fouch, T.D., Lawton, T.F., Nichols, D.J., Cashion, W.B., Cobban, W.A., 1983. Patterns and timing of synorogenic sedimentation in Upper Cretaceous rocks of central and northeast Utah. In: Reynolds, M.W., Dolly, E.D. (Eds.), Mesozoic Paleogeography of the West-central United States, Denver, Colorado. Rocky Mountain Section, SEPM, pp. 305–336.

Gomez-Veroiza, C.A., Steel, R.J., 2010. Iles clastic wedge development and sediment partitioning within a 300-km fluvial to marine Campanian transect (3 m.y.), Western Interior seaway, southwestern Wyoming and northern Colorado. Am. Assoc. Pet. Geol. Bull. 94, 1349–1377.

Gradstein, F., Ogg, J., Smith, A. (Eds.), 2004. A Geologic Time Scale 2004. Cambridge University Press, pp. 372–379.

Gurnis, M., 1993. Phanerozoic marine inundation of continents driven by dynamic topography above subducting slabs. Nature 364, 589–593.

Hampson, G.J., Gani, M.R., Sharman, K.E., Irfan, N., Bracken, B., 2011. Along-strike and down-dip variations in shallow-marine sequence stratigraphic architecture: Upper Cretaceous Star Point Sandstone, Wasatch Plateau, Central Utah, USA. J. Sediment. Res. 81, 159–184.

Hampson, G.J., Gani, M.R., Sahoo, H., Rittersbacher, A., Irfan, N., Ranson, A., Jewell, T.O., Gani, N.D.S., Howell, J.A., Buckley, S.J., Bracken, B., 2012. Controls on large-scale patterns of fluvial sandbody distribution in alluvial to coastal plain strata: Upper Cretaceous Blackhawk Formation, Wasatch Plateau, Central Utah, USA. Sedimentology 59, 2226–2258.

Haq, B.U., Al-Qahtani, A.M., 2005. Phanerozoic cycles of sea-level change on the Arabian Platform. GeoArabia 10, 127–160.

Haq, B.U., Hardenbol, J., Vail, P.R., 1987. Chronology of fluctuating sea levels since the Triassic (250 million years ago to present). Science 235, 1156–1167.

Heller, P.L., Bowdler, S.S., Chambers, H.P., Coogan, J.C., Hagen, E.S., Shuster, M.W., Winslow, N.S., 1986. Time of initial thrusting in the Sevier orogenic belt, Idaho–Wyoming and Utah. Geology 14, 388–391. http://dx.doi.org/10.1130/0091-7613(1986)14<388:TOITIT>2.0.CO;2.

Hettinger, R.D., Kirschbaum, M.A., 2002. Stratigraphy of the Upper Cretaceous Mancos Shale (Upper Part) and Mesaverde Group in the Southern Part of the Uinta and Piceance Basins, Utah and Colorado. U.S. Geological Survey Geologic Investigations Series, vol. I-2764, pp. 1–22.

Jordan, T.E., 1981. Thrust loads and foreland basin evolution, Cretaceous, western United States. Am. Assoc. Pet. Geol. Bull. 65, 2506–2520.

Kiteley, L.W., 1978. Stratigraphic sections of Cretaceous rocks of the northern Denver Basin, northeastern Colorado and southeastern Wyoming. United States Geological Survey.

Liu, S.F., Nummedal, D., 2004. Late Cretaceous subsidence in Wyoming: Quantifying the dynamic component. Geology 32, 397–400.

Liu, S.F., Nummedal, D., Yin, P.G., Luo, H.J., 2005. Linkage of Sevier thrust episodes and Late Cretaceous megasequences across southern Wyoming (USA). Basin Res. 17, 487–506.

Liu, L., Spasojevic, S., Gurnis, M., 2008. Reconstructing Farallon plate subduction beneath North America back to the Late Cretaceous. Science 322, 934–938.

Liu, S.F., Nummedal, D., Liu, L.J., 2011. Migration of dynamic subsidence across the Late Cretaceous United States Western Interior Basin in response to Farallon plate subduction. Geology 39, 555–558.

Luo, H.J., Nummedal, D., Liu, S.F., 2010. 3-D flexural numerical modeling of foreland basins: an example from the Upper Cretaceous across the southwestern Wyoming. Earth Sci. Front. 17, 128–139.

Mitrovica, J.X., Beaumont, C., Jarvis, G.T., 1989. Tilting of continental interiors by the dynamical effects of subduction. Tectonics 8, 1079–1094.

Müller, R.D., Sdrolias, M., Gaina, C., Steinberger, B., Heine, C., 2008. Long-term sea-level fluctuations driven by ocean basin dynamics. Science 319, 1357–1362.

Pang, M., Nummedal, D., 1995. Flexural subsidence and basement tectonics of the Cretaceous Western Interior basin, United States. Geology 23, 173–176.

Spasojevic, S., Gurnis, M., 2012. Sea level and vertical motion of continents from dynamic earth models since the Late Cretaceous. Am. Assoc. Pet. Geol. Bull. 96, 2037–2064.

Spasojevic, S., Liu, L., Gurnis, M., 2009. Adjoint models of mantle convection with seismic, plate motion and stratigraphic constraints: North America since the Late Cretaceous. Geochem. Geophys. Geosyst. 10, Q05W02.

Weimer, R.J., 1970. Rates of deltaic sedimentation and intra-basin deformation, Upper Cretaceous of Rocky Mountain region. In: Morgan, J.P., Shaver, R.H. (Eds.), Deltaic Sedimentation, Modern and Ancient. In: SEPM Special Publication, vol. 15, pp. 270–292.

Weimer, R.J., 1983. Relation of unconformities, tectonics and sea level changes, Cretaceous of the Denver basin and adjacent areas. In: Reynolds, M.W., Dolly, E.D. (Eds.), Mesozoic Paleogeography of West-Central United States. Rocky Mountain Section SEPM, pp. 359–376.